PNAS RESEARCH ARTICLE | BIOCHEMISTRY

Cotranslational folding and assembly of the dimeric *Escherichia coli* inner membrane protein EmrE

Daphne Mermans[a,1], Felix Nicolaus[a,1], Klara Fleisch[a], and Gunnar von Heijne[a,b,2]

Edited by Donald Engelman, Yale University, New Haven, CT; received April 2, 2022; accepted August 1, 2022

In recent years, it has become clear that many homo- and heterodimeric cytoplasmic proteins in both prokaryotic and eukaryotic cells start to dimerize cotranslationally (i.e., while at least one of the two chains is still attached to the ribosome). Whether this is also possible for integral membrane proteins is, however, unknown. Here, we apply force profile analysis (FPA)—a method where a translational arrest peptide (AP) engineered into the polypeptide chain is used to detect force generated on the nascent chain during membrane insertion—to demonstrate cotranslational interactions between a fully membrane-inserted monomer and a nascent, ribosome-tethered monomer of the *Escherichia coli* inner membrane protein EmrE. Similar cotranslational interactions are also seen when the two monomers are fused into a single polypeptide. Further, we uncover an apparent intrachain interaction between E^{14} in transmembrane helix 1 (TMH1) and S^{64} in TMH3 that forms at a precise nascent chain length during cotranslational membrane insertion of an EmrE monomer. Like soluble proteins, inner membrane proteins thus appear to be able to both start to fold and start to dimerize during the cotranslational membrane insertion process.

membrane protein biogenesis | cotranslational folding | cotranslational dimerization | EmrE

Significance

Many water-soluble proteins are known to fold and even dimerize cotranslationally (i.e., when still attached to the ribosome). However, it has proven difficult to ascertain whether transmembrane α-helices in an integral membrane protein can interact cotranslationally and whether membrane proteins can start to dimerize while still being synthesized. Here, we show that a model *Escherichia coli* inner membrane protein appears to be able to start to fold and dimerize cotranslationally in vivo, suggesting the generality of these cotranslational maturation processes.

It is becoming increasingly clear that many, if not most, cytoplasmic proteins start to fold cotranslationally (i.e., while the growing nascent polypeptide chain is still attached to the ribosome). Such early folding events range from the formation of elements of secondary structure and small protein domains already within the ribosome exit tunnel to folding of larger domains just outside the exit tunnel, with or without the help of chaperones (1, 2). Ribosome profiling experiments in both prokaryotic and eukaryotic cells have further shown that many homo- and heterodimeric cytoplasmic proteins can start to dimerize cotranslationally while one or even both monomers are still attached to the ribosome (3). Cotranslational folding and assembly of soluble proteins thus seem to be common phenomena; however, whether this is also true for integral membrane proteins remains unclear. Individual domains in multidomain membrane proteins, such as the cystic fibrosis transmembrane conductance regulator or the *Escherichia coli* inner membrane protein GlpG, fold mainly cotranslationally (4–7), but to what extent individual transmembrane helices (TMHs) can interact during translocon-mediated membrane insertion and whether ribosome-attached, nascent integral membrane proteins can start to dimerize with already folded partner proteins are still open questions.

To address these issues, we decided to perform an in-depth force profile analysis (FPA) of the cotranslational membrane insertion process of the small multidrug-resistance protein EmrE from *E. coli*. EmrE has four TMHs and is a dual-topology protein (i.e., the monomers integrate into the inner membrane in a 50:50 mixture of N_{in}–C_{in} and N_{out}–C_{out} topologies); oppositely oriented monomers then assemble into antiparallel dimers (8, 9). A recent FPA analysis of EmrE suggested that there may be long-range cotranslational interactions between a conserved Glu residue (E^{14}) in the middle of TMH1 and unidentified residues in TMH2 and TMH3 during membrane insertion (7) and hence, that the monomer might start to fold cotranslationally. Further, given the extensive intersubunit packing interactions between the two monomers in the EmrE dimer (10), we speculated that cotranslational dimerization of EmrE might be possible to observe by FPA.

FPA takes advantage of so-called translational arrest peptides (APs)—short stretches of polypeptide that bind with high affinity in the upper reaches of the ribosome exit tunnel and thereby, arrest translation at a specific codon in the messenger RNA (mRNA) (11). The translational arrest can be overcome if a strong-enough pulling force is exerted on the AP, essentially pulling it out of its binding site in the exit tunnel (12–16). APs can be employed as sensitive "molecular force sensors" to report on various cotranslational events, such as protein folding (17, 18), protein translocation (19, 20), and membrane protein integration (7, 13).

Author affiliations: [a]Department of Biochemistry and Biophysics, Stockholm University, SE-106 91 Stockholm, Sweden; and [b]Science for Life Laboratory Stockholm University, SE-171 21 Solna, Sweden

Author contributions: D.M., F.N., and G.v.H. designed research; D.M., F.N., and K.F. performed research; D.M., F.N., and G.v.H. analyzed data; and D.M., F.N., and G.v.H. wrote the paper.

The authors declare no competing interest.

This article is a PNAS Direct Submission.

[1]D.M. and F.N. contributed equally to this work.

[2]To whom correspondence may be addressed. Email: gunnar@dbb.su.se.

This article contains supporting information online at http://www.pnas.org/lookup/suppl/doi:10.1073/pnas.2205810119/-/DCSupplemental.

Published August 22, 2022.

Using FPA, we have now identified a residue in EmrE TMH3 (S^{64}) that appears to form a specific interaction with E^{14} in TMH1 at a precise point during the cotranslational membrane insertion process. We also show that TMH4 in one EmrE monomer can interact cotranslationally with TMH4 in a second already fully membrane-inserted monomer and similarly, that the TMH4 TMHs in a construct where two EmrE monomers have been fused into one polypeptide can interact cotranslationally. Cotranslational folding and dimerization events are thus not restricted to soluble proteins but can also be observed in integral membrane proteins.

Results

FPA. FPA is based on the ability of APs to bind in the upper parts of the ribosome exit tunnel and thereby, pause translation when their last codon is in the ribosomal A site (11). The duration of an AP-induced pause is reduced in proportion to pulling forces exerted on the nascent chain (14, 21) (i.e., APs can act as force sensors) and can be tuned by mutation to react to different force levels (22). In an FPA experiment, a series of constructs is made in which a force-generating sequence element (e.g., a TMH) is placed an increasing number of residues away from an AP [here, we use the AP from *E. coli* SecM (23)], which in turn, is followed by a C-terminal tail (in Fig. 1*A*, construct lengths are denoted by *N*, the number of residues from the N-terminal end of the protein to the C-terminal end of the AP). In constructs where a TMH engages in an interaction that generates a strong-enough pulling force *F* on the nascent chain at the point when the ribosome reaches the last codon of the AP, pausing will be prevented, and mostly full-length (FL) protein will be produced during a short pulse with [^{35}S]-Met (Fig. 1 *B*, *Left*). In contrast, in constructs where little force is exerted on the AP, pausing will be efficient, and more of the shorter, arrested form of the protein will be produced (Fig. 1 *B*, *Right*). The fraction of FL protein produced $f_{FL} = I_{FL}/(I_{FL} + I_A)$, where I_{FL} and I_A are the intensities of the bands representing the FL (*FL*) and arrested (*A*) species on an SDS-PAGE gel (Fig. 1*C*; *SI Appendix*, Fig. S1 shows SDS-PAGE gels of all constructs analyzed in this study), can, therefore, be used as a proxy for *F* in a given construct (21, 24, 25). A plot of f_{FL} vs. *N*—a force profile (FP)—thus can provide a detailed picture of the cotranslational process in question, as reflected in the variation in the force exerted on the nascent chain during translation (Fig. 1*D*; *SI Appendix*, Table S1 shows numerical f_{FL} values for all constructs). FPs can be recorded with up to single-residue resolution by increasing *N* in steps of one residue (corresponding to a lengthening of the nascent chain by ∼3 Å).

Cotranslational Interactions between TMH1 and TMH3 in the EmrE Monomer. In our recent study of the cotranslational membrane insertion of EmrE(C_{out}) (7)—a mutant version of EmrE that inserts only with N_{out}–C_{out} orientation (9)—we found that

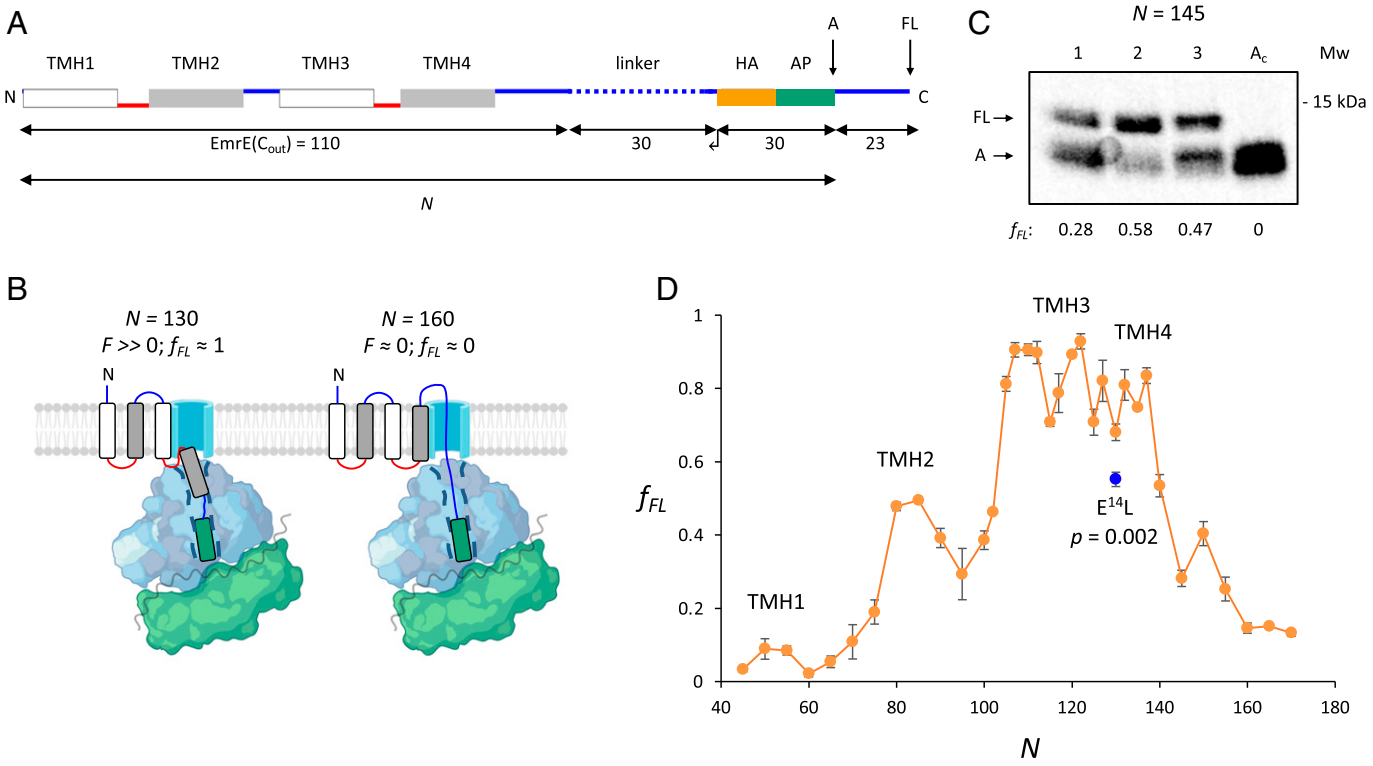

Fig. 1. The FPA. (*A*) Basic EmrE(C_{out}) construct. To obtain an FP, EmrE(C_{out}) is shortened stepwise from the C-terminal end of the LepB-derived linker (dotted), as indicated by the arrow. Cytoplasmic (red) and periplasmic (blue) loops and lengths of FL EmrE(C_{out}), linker, hemagglutinin tag and arrest peptide (HA + AP), and C-terminal tail are indicated. Construct lengths are denoted by *N*, the number of residues between the N-terminal end of EmrE(C_{out}) and the C-terminal end of the AP. Since the 30-residue HA + AP segment is constant in all constructs, the FP reflects nascent chain interactions occurring mainly outside the ribosome exit tunnel. (*B*) At construct length *N* = 130 residues, TMH4 is starting to integrate into the membrane, generating a high pulling force on the nascent chain. At *N* = 160 residues, TMH4 has finished integrating into the membrane and generates little pulling force. (*C*) SDS-PAGE gel showing [^{35}S]-Met–labeled and immunoprecipitated EmrE(C_{out}) (*N* = 145; lane 1), EmrE(C_{out}) (*N* = 145) produced in the presence of coexpressed EmrE(C_{in}) (lane 2), and EmrE(C_{out}) (*N* = 145) produced in the presence of coexpressed EmrE(C_{in};$G^{90}P$ + $G^{97}P$) (lane 3). Control construct A_C has a stop codon replacing the last Pro codon in the AP in EmrE(C_{out}) (*N* = 145; lane 4). The positions of molecular weight (Mw) markers and of FL (*FL*) and arrested (*A*) products on the gel are shown, and average fraction FL (f_{FL}) values are indicated below the lanes. (*D*) FP for EmrE(C_{oot}) (orange). The peaks corresponding to the membrane insertion of TMH1 to TMH4 are indicated (7). Error bars indicate SEM values. The f_{FL} value for construct EmrE(C_{out};E^{14}L) (*N* = 130; the blue data point) is significantly different from the corresponding value for EmrE(C_{out}) (*N* = 130; *P* = 0.002, two-sided Student's *t* test). Sequences for all constructs used in this study are listed in *SI Appendix*, *SI Text*, and all f_{FL} values are in *SI Appendix*, Table S1. Panel *D* is adapted from ref. 7, which is licensed under CC BY 4.0.

mutation of the key functional residue E^{14} in TMH1 to Leu gave rise to significant changes in the FP at three specific nascent chain lengths: $N = 85$, 115, and 130 residues. We decided to focus on the $N = 130$ construct (Fig. 1*D*) as mutation of E^{14} to a hydrophobic (Leu, Ala) but not a polar or charged (Gln, Asp) residue led to a significant reduction in the f_{FL} value at $N = 130$ (7), suggesting the formation of a polar interaction between E^{14} and some other residue in the protein when the nascent chain reaches an overall length of $N = 130$ residues. At this chain length, TMH4 (residues 88 to 103) is about to begin inserting into the membrane, and TMH3 (residues 56 to 78) should just have reached its membrane-spanning disposition with its C-terminal end located ~50 residues away from the peptidyl transferase center (PTC) (Fig. 1 *B*, *Left*). In the EmrE dimer, TMH1 is sandwiched between TMH2 and TMH3 in each monomer (Fig. 2*A*). We, therefore, considered potentially hydrogen-bonding residues in TMH3 (Y^{60}, W^{63}, S^{64}, W^{76}) (Fig. 2*A*) as the best candidates for making a specific interaction with E^{14} at $N = 130$ residues. These four residues were individually mutated to Ala both in EmrE(C_{out}) and in EmrE(C_{out};E^{14}L).

In general, in the absence of specific interactions between TMH3 and upstream TMHs, polar-to-hydrophobic mutations in TMH3 are expected to increase the pulling force generated during its membrane insertion (13), leading to increases in f_{FL}. As seen in Fig. 2*B*, when made in the EmrE(C_{out};E^{14}L) background (blue bars), the Y^{60}A mutation significantly increases f_{FL} at $N = 130$ residues ($P = 0.04$), and none of the other mutations reduce f_{FL}. In contrast, three of the four mutations tend to decrease f_{FL} when made in the EmrE(C_{out}) background (orange bars). The strongest reduction is seen for S^{64}A ($P = 0.02$), which reduces f_{FL} at $N = 130$ residues to approximately the same extent as does the E^{14}L mutation in TMH1 (indicated by the blue line). The double mutation E^{14}L + S^{64}A (blue bar at S^{64}A) has no further effect on f_{FL}. These results suggest that a stabilizing interaction is formed between E^{14} in TMH1 and S^{64} in TMH3 at $N = 130$ residues. Indeed, assuming that TMH1 to TMH3 in the monomer can adopt a structure similar to that seen in the dimer, S^{64} is well placed to interact with E^{14}, as seen in Fig. 2*A*.

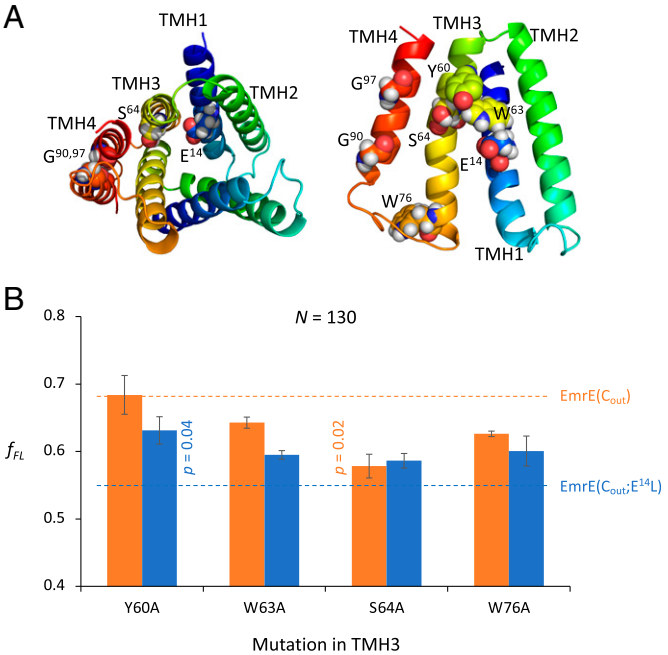

Fig. 2. Identification of cotranslationally interacting residues in EmrE(C_{out}). (*A*) The EmrE dimer (*Left*) and one monomer (*Right*; Protein Data Bank ID code 7MH6) (10). E^{14}, Y^{60}, W^{63}, S^{64}, W^{76}, G^{90}, and G^{97} are shown in space-fill representation. (*B*) f_{FL} values for TMH3 mutations in EmrE(C_{out}) (orange bars) and EmrE(C_{out};E^{14}L) (blue bars) at $N = 130$ residues. The orange and blue lines indicate the f_{FL} values for EmrE(C_{out}) and EmrE(C_{out};E^{14}L) , respectively, at $N = 130$ residues (*c.f.*, Fig. 1*D*). Error bars indicate SEM values ($n \geq 3$) (*SI Appendix*, Table S1). The *P* values for EmrE(C_{out};E^{14}L,Y^{60}A) compared with EmrE(C_{out};E^{14}L) and for EmrE(C_{out};S^{64}A) compared with EmrE(C_{out}), are shown. *P* values were calculated by a two-sided Student's *t* test.

Cotranslational Assembly of the EmrE Dimer. Many soluble cytoplasmic proteins can form both homo- and heterodimers while one of the partner proteins is still being translated (3). Here, we wanted to ascertain whether this is also possible for EmrE that assembles into an antiparallel 4 + 4 TMH homodimer in the inner membrane (10, 26, 27) (Fig. 2*A*).

It has been shown that efficient dimerization of EmrE depends critically on a tight interaction between the TMH4 helices in the two monomers (28), and we, therefore, focused our attention on the part of the FP that reports on the membrane insertion of TMH4 (i.e., $N \sim 130$ to 170 residues) (*c.f.*, Fig. 1*D*). In a first set of experiments, we recorded an FP for EmrE(C_{out}) while coexpressing an oppositely oriented EmrE(C_{in}) version that is known to dimerize efficiently with EmrE(C_{out}) (9, 29, 30) (Fig. 3*A*). Indeed, as shown in Fig. 3*B*, the presence of EmrE(C_{in}) causes a shoulder in the EmrE(C_{out}) FP in the region $N \sim 140$ to 150 residues (magenta data points) where f_{FL} is significantly increased compared with the EmrE(C_{out}) FP (orange data points), suggesting a cotranslational interaction between TMH4 in the nascent EmrE(C_{out}) subunit and the already synthesized EmrE(C_{in}). We further recorded an FP for EmrE(C_{out}) with coexpression of a version of EmrE(C_{in}) carrying Gly → Pro mutations in positions 90 and 97 in TMH4 (Fig. 2*A*) that are known to strongly but not completely destabilize the heterodimer (28, 31). Indeed, the EmrE(C_{out}) FP obtained while coexpressing EmrE(C_{in};G^{90}P + G^{97}P) (light blue data points) was closer to the original EmrE(C_{out}) FP obtained in the absence of coexpressed EmrE(C_{in}). Whether the residual dimerization seen previously for the G^{90}P and G^{97}P mutants (28, 31) can fully explain the remaining differences between the EmrE(C_{out}) FPs obtained with and without coexpression of EmrE(C_{in};G^{90}P + G^{97}P) is unclear; we note, however, that in the experiments in Fig. 3, the G^{90}P + G^{97}P mutation is present only in the EmrE(C_{in}) subunit, possibly leading to a slightly more stable heterodimer than when the mutation is present in both subunits.

To ascertain whether the cotranslational interaction requires that EmrE(C_{in}) is expressed from the same mRNA as EmrE(C_{out}) (i.e., in *cis*), we modified the pET-Duet-1 plasmid used to coexpress EmrE(C_{in}) with EmrE(C_{out}). pET-Duet-1 has two T7 promoters but no intervening transcriptional terminator, and we, therefore, recorded two additional FPs, one in which the second T7 promoter, located upstream of the EmrE(C_{out}) open reading-frame (ORF), was deleted (ΔT7-2) and one in which the strong tripartite tZ terminator (32) was inserted between the EmrE(C_{in}) ORF and the second T7 promoter (*SI Appendix*, Fig. S2). The two FPs were essentially identical to each other and to the original EmrE(C_{in}) + EmrE(C_{out}) FP. Hence, the cotranslational interaction between EmrE(C_{in}) and EmrE(C_{out}) is seen regardless of whether the two subunits are expressed in *cis* or in *trans*.

Finally, we recorded an FP for a fusion construct between EmrE(C_{in}) and EmrE(C_{out}) with an extra TMH inserted between EmrE(C_{in}) and EmrE(C_{out}) (in order to maintain their antiparallel orientations in the membrane) (Fig. 3*C*). This fusion construct is known to be able to form an active intramolecular C_{in} + C_{out} "dimer" (29). The presence of EmrE(C_{in}), now covalently fused to the N terminus of EmrE(C_{out}), caused an even

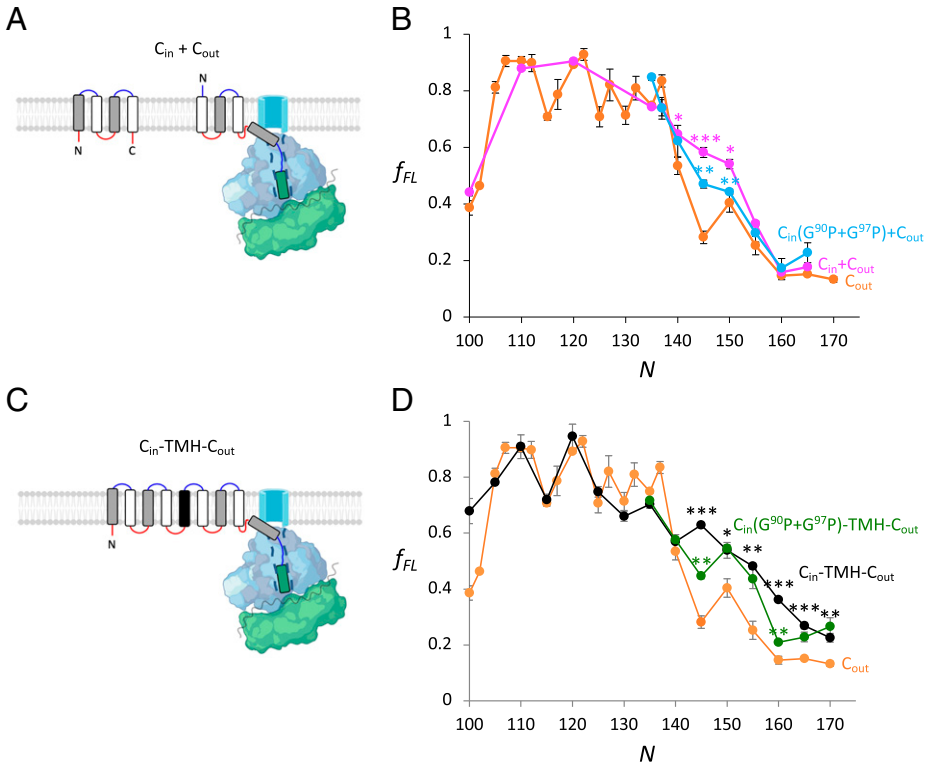

Fig. 3. Cotranslational assembly of the EmrE dimer. (*A*) Setup to obtain an FP for EmrE(C_{out}) while coexpressing EmrE(C_{in}). (*B*) FPs for EmrE(C_{out}) (orange), EmrE(C_{out}) with coexpressed EmrE(C_{in}) (magenta), and EmrE(C_{out}) with coexpressed EmrE(C_{in};$G^{90}P$ + $G^{97}P$) (light blue). *P* values were calculated by a two-sided Student's *t* test comparing the EmrE(C_{out}) data points with those for EmrE(C_{out}) with coexpressed EmrE(C_{in}) (magenta stars) and by comparing the data points for EmrE(C_{out}) with coexpressed EmrE(C_{in}) with those for EmrE(C_{out}) with coexpressed EmrE(C_{in};$G^{90}P$ + $G^{97}P$) (light blue stars). *$P < 0.05$; ** ≤ 0.01; ***$P \leq 0.001$. (*C*) Setup to obtain an FP for an EmrE(C_{in})-TMH-EmrE(C_{out}) fusion construct in which a TMH of composition 7L/12A (black) was included to maintain the opposite orientations of the EmrE(C_{in}) and EmrE(C_{out}) moieties. *N* values were counted from the N-terminal residue of EmrE(C_{out}). (*D*) FPs for fused EmrE(C_{in})-TMH-EmrE(C_{out}) (black), EmrE(C_{out}) (orange), and fused EmrE(C_{in};$G^{90}P$ + $G^{97}P$)-TMH-EmrE(C_{out}) (green). *P* values were calculated comparing the two latter sets of data points with those of EmrE(C_{in})-TMH-EmrE(C_{out}). In all cases, the FPs are for the EmrE(C_{out}) subunit. Error bars indicate SEM values ($n \geq 3$). *$P < 0.05$; **$P \leq 0.01$; ***$P \leq 0.001$.

more conspicuous shoulder in the EmrE(C_{out}) FP (Fig. 3*D*, black data points; *SI Appendix*, Fig. S3 shows the full FP, including the TMH1 to TMH2 region). Again, introduction of the $G^{90}P$ + $G^{97}P$ double mutation in the fused EmrE(C_{in}) part partially reverted this effect (Fig. 3*D*, green data points).

We conclude that the presence of EmrE(C_{in}) during expression of EmrE(C_{out}) gives rise to a clear increase in the f_{FL} values in the $N \sim$ 140- to 150-residues region of the FP (and in an even longer region when the two subunits are fused together). The $G^{90}P$ + $G^{97}P$ mutation in EmrE(C_{in}) TMH4 reduces this effect. According to our earlier work, EmrE(C_{out}) TMH4 starts to insert into the membrane at $N \sim$ 132 residues and stops generating a pulling force on the nascent chain at $N \sim$ 150 residues when the C-terminal end of TMH4 is ~45 residues away from the PTC (7), i.e., the cotranslational interaction seen between EmrE(C_{in}) and EmrE(C_{out}) corresponds to the final steps in the membrane insertion of TMH4. The cotranslational interaction seen in the FP recorded for the fused subunits extends beyond this point, suggesting that other presumably weaker interactions between the two subunits also come into play in this case.

Discussion

Thanks to the high resolution and sensitivity of FPA, we have been able to identify the cotranslational formation of what appears to be a specific interaction between two EmrE residues—E^{14} in TMH1 and S^{64} in TMH3—at the point when TMH3 is just completing its insertion into the inner membrane. The interaction is seen as a small increase in f_{FL} at N = 130 residues, which disappears when either E^{14} or S^{64} is mutated to a nonpolar residue. Thus, TMH1 and TMH3 appear to interact cotranslationally within the context of the SecYEG translocon. We have also found that the EmrE antiparallel dimer can start to assemble in the inner membrane while one of the two monomers is still attached to the ribosome (albeit by an artificial C-terminal tether). The first clear signal of dimerization is seen at $N \sim$ 145 residues (at which point the C-terminal end of TMH4 is ~40 residues from the PTC), corresponding to a situation where TMH4 in the EmrE(C_{out}) monomer is not yet fully inserted into the membrane and must still be in or in the immediate vicinity of the SecYEG translocon. Thus, EmrE(C_{in}) monomers must have access to the SecYEG translocon at this point, which may not be so surprising in the case of the EmrE(C_{in})-TMH-EmrE(C_{out}) fusion construct but is more remarkable in the case of coexpressed EmrE(C_{in}) and EmrE(C_{out}).

More generally, our results show that, just like cytoplasmic proteins (3), inner membrane proteins appear to be able to undergo cotranslational folding and dimerization, adding another level of complexity to the basic two-stage model for membrane protein folding (33, 34).

Materials and Methods

Key resources are shown in Table 1.

Enzymes and Chemicals. Enzymes and other reagents were purchased from Thermo Fisher Scientific, New England Biolabs, and Sigma-Aldrich. Oligonucleotides were ordered from Eurofins Genomics. L-[^{35}S]-methionine was provided

Table 1. Key resources

Reagent type (species) or resource	Designation	Source	Identifiers	Additional information
Strain, strain background (*E. coli*)	BL21(DE3)	Sigma-Aldrich	CMC0016	Electrocompetent cells
Other	Rifampicin	Sigma-Aldrich	R3501	Used for inhibition of bacterial RNA polymerase during expression
Other	Protein G-agarose	Roche	11243233001	Resin used for immunoprecipitation
Antibody	Anti-HA.11 epitope tag antibody (mouse monoclonal) immunoglobulin G	BioLegend	Catalog no. 901533	Used for immunoprecipitation (1 μL of 1 mg/mL, diluted 1:820)
Recombinant DNA reagent	pET-Duet-1 (plasmid)	Novagen	Catalog no. 71146	Expression plasmid
Commercial assay, kit	GeneJET Plasmid miniprep kit	Thermo Fisher Scientific (Research Resource Identifier RRID: SCR_008452)	Catalog no. 0502	Used to purify plasmids
Chemical compound, drug	^{35}S-methionine	Perkin-Elmer	Catalog no. NEG009T001MC	[^{35}S]-Met is incorporated into the protein during in vitro and in vivo translation and aids detection by phosphorimaging
Software, algorithm	EasyQuant	Developed in house (13)		Used to quantify relative fraction FL of translated protein from SDS-PAGE

by PerkinElmer. Anti-HA tag antibody (mouse monoclonal) was obtained from BioLegend.

Cloning and Mutagenesis. The previously described pET-Duet-1 plasmid with N_{out}–C_{out}-oriented EmrE(C_{out}) followed by a variable LepB-derived linker sequence (between 4 and 34 residues), the 9-residue-long hemagglutinin (HA) tag, the 17-residue-long *E. coli* SecM AP, and a 23-residue-long C-terminal tail in multiple cloning site 2 (MCS2) were used to make all constructs in this study (7, 9). To generate the fused dimer construct, the previously described 9TMH-EmrE (C_{in}-TMH-C_{out}) construct was cloned in place of EmrE(C_{out}) in MCS2 of pET-Duet-1 using Gibson assembly (29, 35). For coexpression of EmrE(C_{in}) with EmrE(C_{out}), the gene encoding the N_{in}–C_{in}-oriented EmrE(C_{in}) version was engineered into MCS1 of pET-Duet-1 harboring EmrE(C_{out}) in MCS2 (9). Ordered gene fragments were used to introduce the double mutation $G^{90}P + G^{97}P$ into EmrE(C_{in}). Point mutations in EmrE(C_{out}) and deletion of the T7 promoter-2 (32) were done by performing site-specific DNA mutagenesis. The tZ terminator (32) was inserted 25 bp downstream of the EmrE(C_{in}) stop codon by Gibson assembly. All cloning and mutagenesis products were confirmed by DNA sequencing. EmrE sequences and the pET-Duet-1 versions used in this study are summarized in *SI Appendix*, *SI Text*. The plasmid map in *SI Appendix*, Fig. S2 was generated using SnapGene.

In Vivo Pulse-Labeling Analysis. Induction of protein expression (1 mM isopropyl β-d-1-thiogalactopyranoside, 10 min) followed by [^{35}S]-Met pulse labeling (2 min) of BL21 (DE) cells harboring pET-Duet-1 constructs encoding the different EmrE versions and immunoprecipitation using an antibody directed against the HAtag were carried out as previously described (7). In order to detect tag-less EmrE(C_{in}) (*SI Appendix*, Fig. S2), expression from the pET-Duet-1 plasmids carrying EmrE(C_{in}) in MCS1 was performed using rifampicin to inhibit endogenous transcription (36). In brief, cultures were incubated with 0.2 mg/mL rifampicin after induction and shaken for 15 min at 37 °C before radiolabeling. Samples were precipitated, washed, and immediately solubilized in sodium dodecyl sulfate (SDS) sample buffer followed by incubation with Ribonuclease A and sodium dodecyl sulfate polyacrylamide gel electrophoresis (SDS-PAGE) analysis.

Radiolabeled proteins were detected by exposing dried gels to phosphorimaging plates, which were scanned in a Fuji FLA-3000 scanner. Band-intensity profiles were obtained using the FIJI (ImageJ) software and quantified with our in-house software EasyQuant. A_c and/or FL_c controls were included in the SDS-PAGE analysis for constructs where the identities of the *A* and *FL* bands were not immediately obvious on the gel. Data were collected from at least three independent biological replicates, and averages and SEMs were calculated. Statistical significance was calculated using a two-sided Student's *t* test.

Data, Materials, and Software Availability. All study data are included in the article and/or *SI Appendix*.

ACKNOWLEDGMENTS. We thank Dr. Gerald Striedner (the University of Natural Resources and Life Science, Vienna) for advice on the tZ terminator and Dr. Rickard Hedman (Stockholm University) for programming and maintenance of the EasyQuant software. This work was supported by Marie Curie Initial Training Network Grant Horizon 2020 ProteinFactory 642863 (to F.N.), Knut and Alice Wallenberg Foundation Grant 2017.0323 (to G.v.H.), Novo Nordisk Fund Grant NNF18OC0032828 (to G.v.H.), and Swedish Research Council Grant 2020-03238 (to G.v.H.).

1. M. Liutkute, E. Samatova, M. V. Rodnina, Cotranslational folding of proteins on the ribosome. *Biomolecules* **10**, E97 (2020).
2. A. M. E. Cassaignau, L. D. Cabrita, J. Christodoulou, How does the ribosome fold the proteome? *Annu. Rev. Biochem.* **89**, 389–415 (2020).
3. J. Koubek, J. Schmitt, C. V. Galmozzi, G. Kramer, Mechanisms of cotranslational protein maturation in bacteria. *Front. Mol. Biosci.* **8**, 689755 (2021).
4. B. Kleizen, T. van Vlijmen, H. R. de Jonge, I. Braakman, Folding of CFTR is predominantly cotranslational. *Mol. Cell* **20**, 277–287 (2005).
5. S. J. Kim, W. R. Skach, Mechanisms of CFTR folding at the endoplasmic reticulum. *Front. Pharmacol.* **3**, 201 (2012).
6. L. Ellgaard, N. McCaul, A. Chatsisvili, I. Braakman, Co- and post-translational protein folding in the ER. *Traffic* **17**, 615–638 (2016).
7. F. Nicolaus *et al.*, Residue-by-residue analysis of cotranslational membrane protein integration in vivo. *eLife* **10**, e64302 (2021).
8. Y. J. Chen *et al.*, X-ray structure of EmrE supports dual topology model. *Proc. Natl. Acad. Sci. U.S.A.* **104**, 18999–19004 (2007).

9. M. Rapp, S. Seppälä, E. Granseth, G. von Heijne, Emulating membrane protein evolution by rational design. *Science* **315**, 1282–1284 (2007).
10. A. A. Kermani *et al.*, Crystal structures of bacterial small multidrug resistance transporter EmrE in complex with structurally diverse substrates. *eLife* **11**, e76766 (2022).
11. K. Ito, S. Chiba, Arrest peptides: Cis-acting modulators of translation. *Annu. Rev. Biochem.* **82**, 171–202 (2013).
12. M. E. Butkus, L. B. Prundeanu, D. B. Oliver, Translocon "pulling" of nascent SecM controls the duration of its translational pause and secretion-responsive secA regulation. *J. Bacteriol.* **185**, 6719–6722 (2003).
13. N. Ismail, R. Hedman, N. Schiller, G. von Heijne, A biphasic pulling force acts on transmembrane helices during translocon-mediated membrane integration. *Nat. Struct. Mol. Biol.* **19**, 1018–1022 (2012).
14. D. H. Goldman *et al.*, Ribosome. Mechanical force releases nascent chain-mediated ribosome arrest in vitro and in vivo. *Science* **348**, 457–460 (2015).
15. F. Di Palma *et al.*, Probing interplays between human XBP1u translational arrest peptide and 80s ribosome. *J. Chem. Theory Comput.* **18**, 1905–1914 (2022).
16. M. H. Zimmer, M. J. M. Niesen, T. F. Miller III, Force transduction creates long-ranged coupling in ribosomes stalled by arrest peptides. *Biophys. J.* **120**, 2425–2435 (2021).
17. O. B. Nilsson *et al.*, Cotranslational protein folding inside the ribosome exit tunnel. *Cell Rep.* **12**, 1533–1540 (2015).
18. M. Liutkute, M. Maiti, E. Samatova, J. Enderlein, M. V. Rodnina, Gradual compaction of the nascent peptide during cotranslational folding on the ribosome. *eLife* **9**, e60895 (2020).
19. N. Ismail, R. Hedman, M. Lindén, G. von Heijne, Charge-driven dynamics of nascent-chain movement through the SecYEG translocon. *Nat. Struct. Mol. Biol.* **22**, 145–149 (2015).
20. H. Sandhu *et al.*, Cotranslational translocation and folding of a periplasmic protein domain in *Escherichia coli*. *J. Mol. Biol.* **433**, 167047 (2021).
21. G. Kemp, O. B. Nilsson, P. Tian, R. B. Best, G. von Heijne, Cotranslational folding cooperativity of contiguous domains of α-spectrin. *Proc. Natl. Acad. Sci. U.S.A.* **117**, 14119–14126 (2020).
22. F. Cymer, R. Hedman, N. Ismail, G. von Heijne, Exploration of the arrest peptide sequence space reveals arrest-enhanced variants. *J. Biol. Chem.* **290**, 10208–10215 (2015).
23. H. Nakatogawa, K. Ito, Secretion monitor, SecM, undergoes self-translation arrest in the cytosol. *Mol. Cell* **7**, 185–192 (2001).
24. M. J. M. Niesen, A. Müller-Lucks, R. Hedman, G. von Heijne, T. F. Miller III, Forces on nascent polypeptides during membrane insertion and translocation via the Sec translocon. *Biophys. J.* **115**, 1885–1894 (2018).
25. S. E. Leininger, F. Trovato, D. A. Nissley, E. P. O'Brien, Domain topology, stability, and translation speed determine mechanical force generation on the ribosome. *Proc. Natl. Acad. Sci. U.S.A.* **116**, 5523–5532 (2019).
26. I. Ubarretxena-Belandia, J. M. Baldwin, S. Schuldiner, C. G. Tate, Three-dimensional structure of the bacterial multidrug transporter EmrE shows it is an asymmetric homodimer. *EMBO J.* **22**, 6175–6181 (2003).
27. M. Rapp, E. Granseth, S. Seppälä, G. von Heijne, Identification and evolution of dual-topology membrane proteins. *Nat. Struct. Mol. Biol.* **13**, 112–116 (2006).
28. Y. Elbaz, T. Salomon, S. Schuldiner, Identification of a glycine motif required for packing in EmrE, a multidrug transporter from *Escherichia coli*. *J. Biol. Chem.* **283**, 12276–12283 (2008).
29. P. Lloris-Garcerá, S. Seppälä, J. S. Slusky, M. Rapp, G. von Heijne, Why have small multidrug resistance proteins not evolved into fused, internally duplicated structures? *J. Mol. Biol.* **426**, 2246–2254 (2014).
30. S. Seppälä, J. S. Slusky, P. Lloris-Garcerá, M. Rapp, G. von Heijne, Control of membrane protein topology by a single C-terminal residue. *Science* **328**, 1698–1700 (2010).
31. N. Fluman, V. Tobiasson, G. von Heijne, Stable membrane orientations of small dual-topology membrane proteins. *Proc. Natl. Acad. Sci. U.S.A.* **114**, 7987–7992 (2017).
32. J. Mairhofer, A. Wittwer, M. Cserjan-Puschmann, G. Striedner, Preventing T7 RNA polymerase read-through transcription-A synthetic termination signal capable of improving bioprocess stability. *ACS Synth. Biol.* **4**, 265–273 (2015).
33. D. M. Engelman *et al.*, Membrane protein folding: Beyond the two stage model. *FEBS Lett.* **555**, 122–125 (2003).
34. J. L. Popot, D. M. Engelman, Helical membrane protein folding, stability, and evolution. *Annu. Rev. Biochem.* **69**, 881–922 (2000).
35. D. G. Gibson *et al.*, Enzymatic assembly of DNA molecules up to several hundred kilobases. *Nat. Methods* **6**, 343–345 (2009).
36. I. Nasie, S. Steiner-Mordoch, S. Schuldiner, Topology determination of untagged membrane proteins. *Methods Mol. Biol.* **1033**, 121–130 (2013).